Lawrence Berkeley National Laboratory

Title

Creation of hollow silica-fiberglass soft ceramics for thermal insulation

Permalink

https://escholarship.org/uc/item/7gp2x8nc

Authors

Liu, Shuo
Dun, Chaochao
Wei, Jilun
et al.

1

Creation of Hollow Silica – Fiberglass Soft Ceramics for Thermal Insulation

4

Shuo Liu[a], Chaochao Dun[b], Jilun Wei[a], Lu An[c], Shenqiang Ren[c,d,e], Jeffrey J. Urban[b], and Mark T. Swihart[a,d]*

7

8

[a]Department of Chemical and Biological Engineering, University at Buffalo (SUNY), Buffalo, NY 14260 USA
[b]The Molecular Foundry, Lawrence Berkeley National Laboratory, Berkeley, CA 94720, USA
[c]Department of Mechanical and Aerospace Engineering, University at Buffalo (SUNY), Buffalo, NY 14260 USA
[d]RENEW Institute, University at Buffalo (SUNY), Buffalo, NY 14260 USA
[e]Department of Chemistry, University at Buffalo (SUNY), Buffalo, NY 14260 USA
*Corresponding author: swihart@buffalo.edu

19

20

21

22

23

Abstract

Hollow-structured materials show promise in thermal insulation because the shell encapsulating gaseous voids can interrupt heat transport pathways. Here, we present two low-cost routes to fabricate hollow silica nanoshells, via gas-phase and liquid-phase methods. The gas-phase synthesis method generates hollow shells by a droplet surface precipitation mechanism in a flame aerosol reactor. The liquid-phase synthesis route forms hollow shells by removal of a carbon template, which is produced by hydrothermal reaction of glucose. Both approaches (gas- and liquid-phase) provide hollow silica with amorphous structure, low thermal conductivity (0.023 and 0.026 W m^{-1} K^{-1}), small particle size (442 and 383 nm), thin shell (35 and 36 nm), and low density (0.015 and 0.033 g cm^{-3}). We employed high shear mechanical mixing to fabricate hollow silica – fiberglass composite ceramics. The resulting three-dimensional network provides the ceramics with robust mechanical elasticity and fire-retardancy while maintaining the low thermal conductivity, dramatically outperforming an analogous material using commercial silica gel in place of the hollow nanoshells. Our findings provide two practical routes to synthesize hollow silica, either of which can be used to manufacture a class of aerosol-fiber soft ceramics for energy-saving applications.

Keywords: Hollow silica; thermal insulation; aerogel ceramic; fiberglass; mechanical flexibility; energy conservation

Introduction

Thermal energy accounts for a major portion of overall energy consumption in our society. Thus, thermal insulation materials, which limit heat flow, play a significant role in thermal energy storage and conservation.[1] In this context, silica aerogel, which limits thermal by confining air in voids created by the aggregated assembly of silica nanoparticles, provides ultralow thermal conductivity ($\approx$ 0.013 W m^{-1} K^{-1}) and is one of the most effective insulation materials for thermal management.[2, 3] However, practical use of silica aerogel is normally limited by its fragile structure and the high cost of its energy-intensive fabrication process involving CO_2 supercritical drying.[4-6] The excellent insulation performance of silica aerogels motivates researches to improve their mechanical properties,[7, 8] lower their production cost,[9, 10] and develop other nanomaterials with similar properties.[11-14] Among them, hollow silica micro/nano-sphere show great promise, due to their low thermal conductivity and density, approaching those of silica aerogels.[15-17]

The voids in hollow silica, similar to those in silica aerogels, interrupt heat transport pathways in both the solid and gas phases.[15, 16] Several strategies have been developed to introduce a hollow void in silica particles, such as use of a sacrificial template,[18] emulsification,[19] and acid etch methods.[20] These liquid-phase synthesis methods enable flexible design of the particle size, shell thickness, and porosity,[21] but often require multi-step batch operations, resulting in laborious production procedures.[22, 23] In contrast, aerosol processes, *i.e.*, gas-phase continuous nanoparticle synthesis methods, are the most common technologies for large-scale production of inorganic powders in industry.[24, 25] Previous studies reported the fabrication of hollow silica

71 microsphere particles using a spray-drying aerosol process, based on a template-

72 free "droplet-to-particle" conversion.[26-28] In general, the "droplet-to-particle"

73 conversion produces hollow voids by precursor droplet evaporation, which leads to

74 a higher solute concentration at the droplet surface than in its interior. As a result,

75 the product precipitates on the droplet surface and grows toward the center,

76 finally resulting in a hollow structure. However, the relatively mild reaction

77 conditions (low temperature and long residence time) usually result in a large

78 particle size and thick shell,[27, 29] relative to the dimensions desired for thermal

79 insulation applications, where small void size and thin shells are desired.[16] In

80 contrast, flame aerosol processes can form nano-sized silica particles via the "gas-

81 to-particle" conversion but that route does not provide a hollow structure.[30-32]

82 Therefore, a novel gas-phase synthesis method, which combines both advantages

83 of spray-drying and flame aerosol processes, and produces hollow silica particles

84 with small size and thin shell, is highly desirable.[33-36]

85

86 Furthermore, assembly of hollow silica particles into bulk materials is necessary for

87 practical use in thermal insulation. Previous studies demonstrated that the hollow

88 silica particles can be directly assembled into self-supported macroscopic colloidal

89 crystals by thermal annealing[37, 38] or sintered to porous ceramics.[39]

90 However, the physical particle aggregation and narrow solid contacts lead to the

91 brittle and stiff nature of such aerogel ceramics, greatly limiting their applications

92 in dynamic and high energy output environments, such isolation of battery packs

93 subject thermal runaway and fireproofing.[8, 40] Simultaneously, the bonding

94 between silica shells generates solid heat transport pathways and increases the

95 thermal conductivity.[16] Blends of hollow silica particles into a polymer matrix to

96 fabricate thermal insulation films can produce robust mechanical properties,[17,

97 41, 42] but the intrinsic high thermal conductivity and low melting point of

98 polymers constrain the potential of this class of materials. Recently, some

99 technologies have been developed to reinforce aerogel particles with fibers

100 (polymer fiber or fiberglass), such as electrospinning,[43] hot pressing,[44] and 3D

101 printing,[45] which can produce both excellent thermal insulation and mechanical

102 properties. For example, incorporation of hollow silica nanoshells into a matrix of

103 polymer fibers by electrospinning can yield flexible insulation composite

104 membranes with low thermal conductivities of 0.0236 W m^{-1} K^{-1}[46] and 0.016 W m^{-1}

105 K^{-1}.[47] However, despite the outstanding potential, these methods still face

106 barriers for practical use due to limited ability to scale up and high energy inputs

107 per quantity of material produced.

108

109 In this study, we adopt a gas-phase synthesis method based on a modified aerosol

110 reactor to produce hollow silica particles with small size and thin, porous shell

111 following an approach we have previously presented.[48] In addition, we also

112 adopt a liquid-phase synthesis route to produce hollow silica particles, using

113 carbon microspheres prepared from glucose by a hydrothermal reaction, as a

114 sacrificial template.[18] Both as-synthesized hollow silicas exhibit much lower

115 thermal conductivity than commercial silica gel. We also report a facile high-shear

116 mechanical mixing method for the large-scale manufacturing of hollow silica –

117 fiberglass soft ceramic insulation materials, without any expensive devices,

118 energy-consuming procedures, or organic chemicals involved. The resulting soft

119 ceramics show an internal structure of a 3D network between connected hollow

120 silica particles and the fiberglass matrix. The hollow silica particles are reasonably

121 assembled together and uniformly distributed on the fiberglass surface, at the

122 same time, while the fiberglass networks are interfaced and further reinforced with

123 hollow silica. Such a synergistic effect improves the mechanical performance while

124 maintaining the low thermal conductivity of hollow silica. This fabrication strategy

125 allows creation of aerogel-fiber composite soft ceramics for thermal management

126 by a low-cost and environmentally friendly route.

127

Experimental section

128

1. Chemicals

129

130 Tetraethyl orthosilicate (TEOS, 98%), hexadecyltrimethylammonium bromide

131 (CTAB, 99+%), and hydrochloric acid solution (37% HCl) were obtained from

132 ACROS ORGANICS. Glucose monohydrate ($C_6H_{12}O_6 \cdot H_2O$) was obtained from SIGMA-

133 ALDRICH. Ethanol (200 proof) was obtained from Decon Labs, Inc. Ammonium

134 hydroxide solution (28.0~30.0% NH_3) was obtained from EMD Millipore. The

135 commercial silica gel (C-SiO_2) was obtained from Aldrich Chemical Company

136 (Catalog No. 28,860-8). The commercial fiberglass was obtained from Unifrax

137 (Grade C-08-F).

138

2. Fabrication of hollow silica particles

139

2.1 G-SiO₂

140

141 The material denoted as G-SiO_2 was produced *via* gas-phase synthesis route in a

142 modified flame aerosol reactor (**Figure S1**). The H_2-rich flame was produced using

143 flows of 17 L/min H_2, 4 L/min O_2, and 7 L/min N_2, which produced a peak

144 temperature of ~800 ºC in the reaction chamber. The precursor solution

145 containing 12.5 g TEOS, varying amounts of CTAB (CTAB: TEOS molar ratios of

146 0.04~0.22), 400 mL H_2O, 100 mL ethanol, and HCl (to reach pH~2) was sent to the

147 nozzle by a peristaltic pump at a flow rate of 300 mL/h. In the reaction chamber,

148 the precursor solution was atomized into droplets, and the hollow silica particles

149 formed from the droplets. Then, the intermediate product was quenched by a high

150 speed N_2 flow (100 L/min) and finally was collected on a PVDF filter membrane (Ø

151 29.3 cm). Finally, the G-SiO_2 was obtained by calcining the intermediate product at

152 500 ºC for 4 hours in air.

153

154 ***2.2 L-SiO$_2$***

155 The material denoted as L-SiO_2 was produced in the liquid phase by a sacrificial

156 template method. The carbon template was synthesized using hydrothermal

157 reaction, where the 60 mL of aqueous glucose solution (0.5~2 M) was placed in a

158 100 mL Teflon-lined stainless-steel autoclave at 180 ºC for 8 hours. For fabricating

159 the hollow L-SiO_2, firstly, 0.4 g of the carbon template was uniformly dispersed in

160 100 mL ethanol, 4 mL H_2O, and 4 mL NH_4OH by sonication in a bath sonicator.

161 Then, TEOS was dissolved in 20 mL ethanol and then added into above carbon

162 suspension, with the TEOS concentration varied from 5~60 g/L in the final mixture.

163 The precursor mixture was magnetically stirred at room temperature for 5 hours to

164 deposit the organosilica on the carbon surface. After that, the intermediate

165 product was separated by vacuum filtration, washed with ethanol, and dried

166 overnight. Finally, the L-SiO_2 was obtained by calcining the intermediate product at

167 500 ºC for 4 hours in air.

168

169 **3. Fabrication of silica-fiberglass soft ceramic**

170 The hollow silica particles and fiberglass were combined via dispersion in water

171 using a high-shear blender, then collecting them by vacuum filtration and pressing

172 to control the final density of the composite. In details, fiberglass and 300 mL H_2O

173 were placed in a high-shear blender (Eapmic 1108A) and mixed for 10 seconds to

174 break the silica fibers. Then, hollow silica particles were added into the blender,

175 such that the total mass of fiberglass and silica particles was 2 g, with varied

176 hollow silica content of 0 to 80 wt.%. This was blended for 15 seconds to fully mix

177 the fiberglass and silica particle. Next, the resulting suspension was placed in an

178 ultrasonic bath (Kendal HB-S-49MHT) and sonicated at ~42 kHz for 20 minutes.

179 After that, the water was removed by vacuum filtration and the solid material was

180 shaped and collected on the filter paper (Whatman 1001-090, 90 mm diameter).

181 The material density was engineered by thermal compression, in which the wet

182 sample was covered by aluminum foil and compressed into different thickness in a

183 tablet machine (PCH-600CG) and kept at 150 ºC for 30 minutes. Finally, it was

184 dried at 70 ºC overnight to form the silica-fiberglass soft ceramic.

185

186 **4. Material characterization**

187 The JEOL 2100-F 200 kV field-emission analytical Transmission Electron Microscope

188 (TEM) was used to obtain the high-angle annular dark-field imaging and element

189 distribution (HAADF-STEM elemental mapping). Another TEM (JEOL JEM 2010) and

190 a Cross-Beam Focused Ion Beam-Scanning Electron Microscopy (SEM) Workstation

191 (Carl Zeiss AURIGA) were used to observe the microscopic structure of samples.

192 The fiberglass composition was measured by Energy Dispersive X-ray

193 Spectroscopy (EDS, Oxford Instruments) in the SEM. Powder X-ray diffraction (XRD,

194 Rigaku Ultima IV) was adopted to determine the crystal structure. Nitrogen

195 physisorption analysis (Micromeritics Tri-Star II) was used to characterize pore

196 structure of silica samples. Fourier Transform Infrared spectroscopy (FTIR, Bruker

197 Vertex 70) and Raman spectroscopy (Renishaw InVia) were used to probe the

198 surface groups of silica samples. Thermo-Gravimetric analysis (TGA, TA

199 instruments DSC SDT Q600) was performed to measure the mass loss of

200 intermediate products. The thermal conductivity measurement was performed

201 with a custom laboratory device following the ASTM C518 standard thermal

202 conductivity procedure, and a polystyrene reference sample was used to calibrate

203 the flux sensor provided by Fluxteq company.[49] An infrared thermal camera

204 (Fotric 225) was used to take the infrared images of soft ceramics on a 360 ºC hot

205 plate. The mechanical flexibility of the soft ceramics was characterized by a

206 universal MTS testing machine.[49]

207

208 **Results and discussion**

209 The hollow G-SiO$_2$ particle was formed by a droplet-to-particle conversion route in

210 an aerosol reactor, as shown in **Figure 1A**. The TEOS solution was atomized to

211 micro-sized droplets by the sonic-velocity stream of hot combustion product gases.

212 Each droplet produces a single nanoshell inside the reaction chamber. In detail,

213 the droplet evaporation increased TEOS concentration to drive organosilica sol-gel

214 process. Here, the evaporation rate (<0.05s) was much faster than the molecular

215 diffusion rate in the droplet, so the TEOS concentration in the droplet surface

216 region was higher than the center. We added the cation surfactant (CTAB) in the

217 precursor to induce porosity in the final structure. When the CTAB concentration

218 exceeded the critical micelle concentration (CMC) during the evaporation process,

219 it would self-assemble into cylindrical micelles that serve as a soft template for

220 pore formation in the organosilica matrix. Finally, removal of the organics in the

221 intermediate product by calcination generated a hollow and porous silica nanoshell

222 structure. The HAADF-STEM elemental mappings clearly reveals the hollow void

223 and silica composition of G-SiO$_2$.

224

225 The hollow L-SiO$_2$ particle was fabricated by a sacrificial template route in the

226 liquid phase, with the hydrothermal carbon as hard-template, as shown in **Figure**

227   **1B**. Glucose molecules underwent dehydration and polymerization in the

228   hydrothermal reaction, forming carbon microspheres.[50] Then, the carbon

229   template was dispersed in a solvent and the TEOS was added into the suspension.

230   In the alkaline environment, organosilica precipitated on the carbon microsphere

231   surface *via* a sol-gel process. Removal of the carbon template and other organics

232   by calcination produced the hollow silica particles. Similarly, the HAADF-STEM

233   elemental mapping clearly shows the hollow void and silica composition of L-SiO$_2$.

234
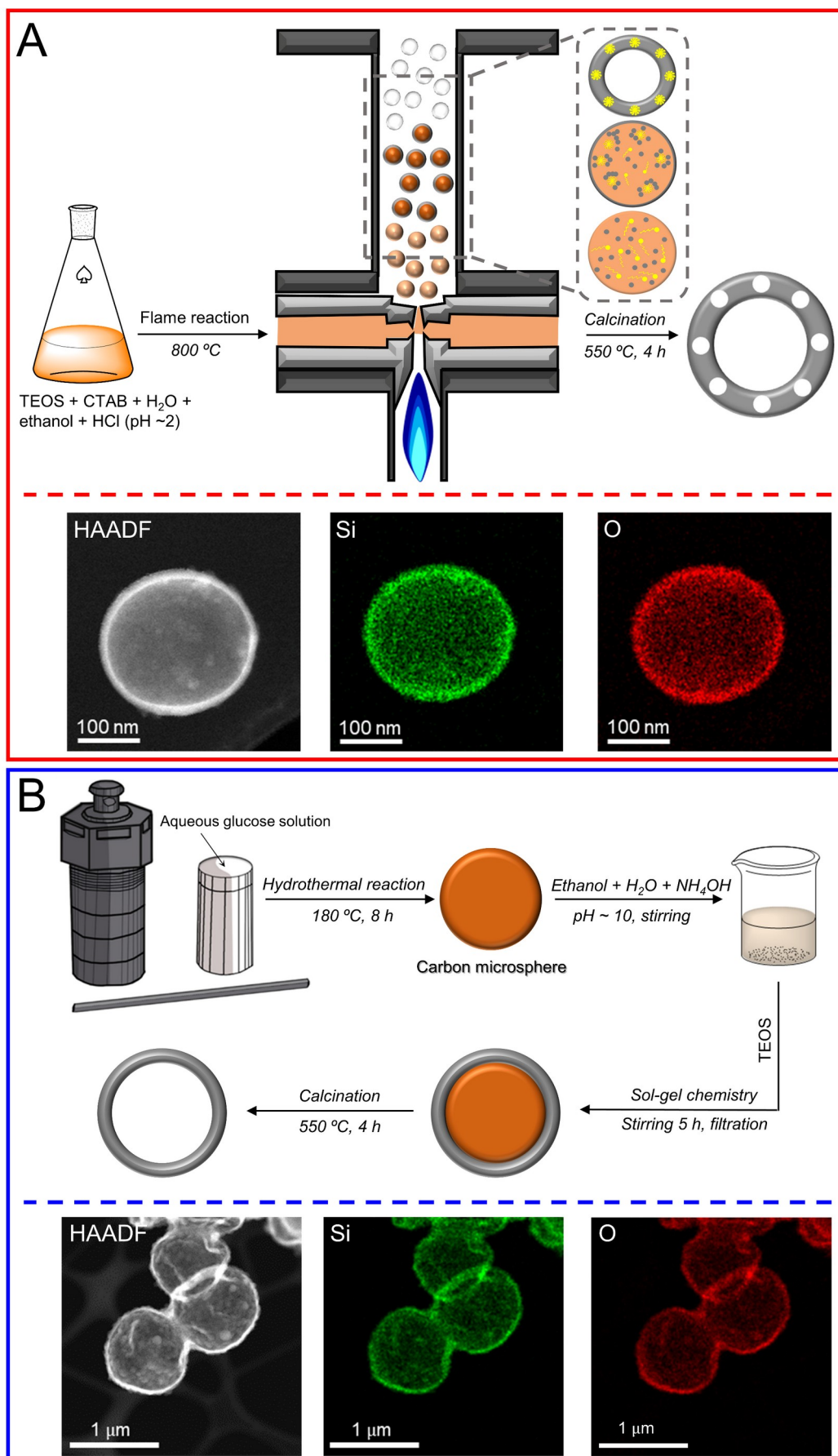
Figure 1. Hollow silica particle formation mechanism and HAADF-STEM element maps. **A.** G-SiO$_2$ fabricated in the gas phase and **B.** L-SiO$_2$ fabricated in the liquid

237 phase.
238 The thermal insulation performance of hollow silica or other aerogels is dependent

239 on multiple factors, such as density, morphology, and porosity. For example, a high

240 porosity with small pore size and the hollow void with thin shell could greatly limit

241 the gas motion, and therefore reduce thermal conductivity. [12, 15] Low density

242 (high porosity) reduces the solid-phase thermal conduction.[51] This research aims

243 to control the key properties of G-SiO$_2$ and L-SiO$_2$ by varying synthesis parameters.

244 In general, materials produced from aerosol synthesis methods often suffer from

245 limited control of morphology and structure, along with inhomogeneous size

246 distribution, due to the violent spray pyrolysis reaction and fast particle formation.

247 [24] Fortunately, the density of G-SiO$_2$ is controllable by adjusting the CTAB: TEOS

248 molar ratio in precursor solution.

249

250 As shown in **Table S1**, upon increasing the CTAB: TEOS molar ratio from 0.04 to

251 0.22, the density of G-SiO$_2$ first decreased then increased. The lowest density of

252 0.015 g/cm^3 was obtained at a CTAB:TEOS molar ratio of 0.08, which also provides

253 the lowest thermal conductivity of 0.023 W/(mK). All four G-SiO$_2$ samples mainly

254 exhibited a hollow and porous nanoshell morphology (**Figure S2A-D**), although

255 some vesical structures were observed in the G-SiO$_2$ fabricated with the 0.08

256 CTAB:TEOS molar ratio (**Figure S3A-B**). More detailed characterization results for

257 the optimized G-SiO$_2$ with the lowest density of 0.015 g/cm^3 are shown in **Figure**

258 **S4**. The XRD pattern demonstrated the amorphous phase of G-SiO$_2$ (**Figure S4A**),

259 in which heat transfer is inhibited by the highly disordered structure resulting in

260 lower thermal conductivity than crystalline materials.[13] The size distribution

261 curve reveals the intrinsic inhomogeneity of the particles generated from such

262 aerosol processes (**Figure S4B**). N$_2$ sorption measurements in **Figure S4C**

263 showed type IV isotherms, consistent with a mesoporous structure. [52] The BJH

adsorption pore size distribution showed narrow pores of 1~5 nm in the wall (**Figure S4D**), which is much smaller than the air molecules mean free path (~68 nm at ambient conditions) which limits heat transfer by intermolecular collisions. [53] Additionally, TGA and FTIR analysis (**Figure S4E-F**) of the intermediate product demonstrated that organic components were removed below 550 ºC, and only SiO_2 remained after calcination, with a few isolated silanol groups.[54]

In contrast to the aerosol synthesis, liquid-phase methods often provide easy morphology control. Here, carbon microspheres were first synthesized in the hydrothermal reaction. As shown in **Figure S5**, the initial glucose aqueous concentration had significant effect on carbon average diameter, and relatively small carbon microsphere size was achieved at ~1 M. Meanwhile, the hollow void size of $L-SiO_2$ depends on the diameter of carbon microsphere, and **Figure S6** exhibits that the board void size of $L-SiO_2$ can be achieved from 300 to 2300 nm by using different carbon templates. **Figure S7** shows the hollow $L-SiO_2$ samples fabricated with various TEOS concentrations from 5 g/L to 60 g/L, which demonstrates that the shell thickness of $L-SiO_2$ can be controlled by the TEOS concentration when carbon amount was fixed. High TEOS concentration often generated thicker shell. In addition, a low TEOS concentration of 5 g/L generated irregular shape, and further increasing TEOS concentration led to a regular and homogeneous hollow nanoshell structure; while a high TEOS concentration of 60 g/L formed undesirable small-size solid particles due to homogenous nucleation in addition to heterogeneous deposition of silica on the carbon template. Detailed properties of $L-SiO_2$ samples are provided in **Table S2**, including apparent density, mean average diameter, average shell thickness and thermal conductivity. As a typical example, the $L-SiO_2$ fabricated with 10 g/L TEOS was selected for further

characterization and application because of its lowest density and thermal conductivity. The XRD pattern demonstrated its amorphous structure (**Figure S8A**), and the size distribution curve reflected its homogeneity (**Figure S8B**). N_2 sorption measurements in **Figure S8C** showed type III isotherms, indicating limited porosity, and the BJH adsorption analysis revealed a broad pore size distribution (**Figure S8D**). TGA and Raman analysis (**Figure S8E-F**) demonstrated that the carbon template was removed below 550 °C. Also, Raman analysis of the intermediate product showed a low D band to G band intensity ratio of 0.33, indicating a high graphitic degree of the carbon microsphere.

We summarize the properties of $G-SiO_2$, $L-SiO_2$, and the commercial silica gel $C-SiO_2$ in **Table 1**, and their TEM and SEM images are shown in **Figure 2**. Both $G-SiO_2$ and $L-SiO_2$ provided hollow nanoparticle structures with thin nanoshells. The hollow shell of $G-SiO_2$ presented a smooth surface with mesopores inside, providing huge specific surface area and pore volume; while the hollow shell of $L-SiO_2$ consisted of aggregated silica nanoparticles, resulting in a rough surface and limited porosity. On the other hand, $L-SiO_2$ showed more uniform particle size. Meanwhile, both $G-SiO_2$ and $L-SiO_2$ exhibited ultralow density and thermal conductivity due to the small hollow void and thin shell, which are comparable to those of silica aerogels prepared by supercritical drying technology, indicating the great potential of these materials in thermal insulation applications. In contrast, although the commercial silica gel ($C-SiO_2$) had amorphous structure and exhibited high porosity due to the mesopores between silica nanoparticles (**Figure S9**), the accumulation of solid matter caused the huge particle size in macroscopy, resulting in the high density and thermal conductivity.

Table 1. Material characterizations of silica aerogels

Samples	G-SiO$_2$	L-SiO$_2$	C-SiO$_2$
Crystallinity	amorphous	amorphous	amorphous
BET surface area (m^2 g^{-1})	665	35	331
Pore volume (cm^3 g^{-1})	0.498	0.165	0.813
Average pore size (nm)	2.92	44.8	7.68
Apparent density (g cm^{-3})	0.015	0.033	0.470
Mean average diameter (nm)	442	383	N.A.
Geometric average diameter (nm)	287	377	N.A.
Average shell thickness (nm)	35.0	36.0	N.A.
Thermal conductivity (W m^{-1} K^{-1})	0.023	0.025	0.046

N.A. Related data is not available.
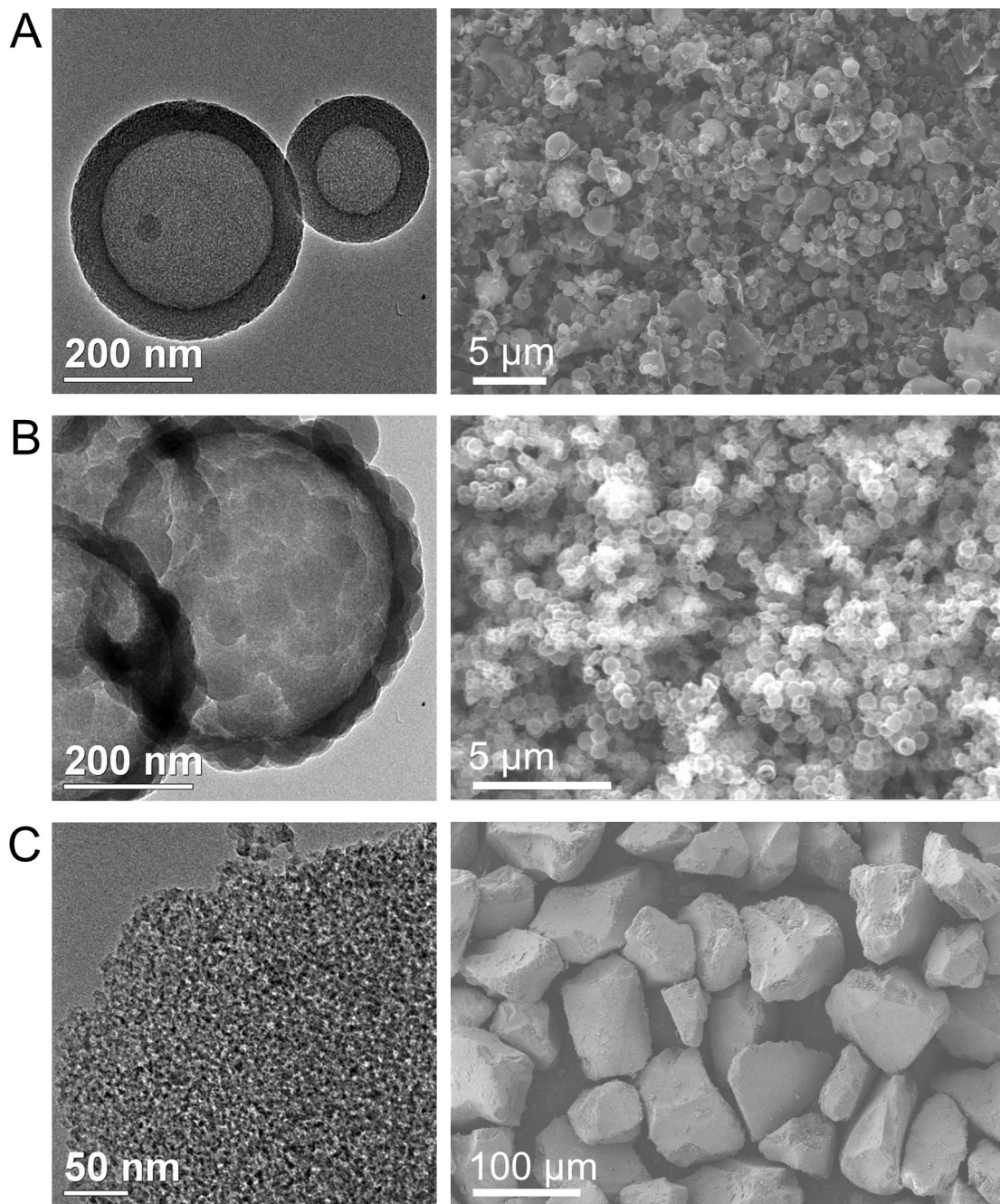
Figure 2. TEM and SEM images of **A.** G-SiO$_2$, **B.** L-SiO$_2$, and **C.** C-SiO$_2$.

For practical use of the hollow silica in thermal insulation, the loose particles must be converted into a bulk material with robust mechanical properties. Fiber reinforcement is a known strategy to assemble silica aerogel powder and overcome its brittleness.[55] We further confirmed here that ceramic fiber can be employed as a scaffold for loading a large amount of hollow silica particles thanks to its high strength and flexibility, low density, thermal stability, and low cost.

324 **Figure S10** shows the basic information of C-08-F glass microfiber (amorphous
325 structure) adopted in this work, with a nominal specific surface area of 2 m^2/g, as
326 well as a nominal fiber diameter of 0.8 μm. As expected, the EDS analysis
327 indicated that the major component of the commercial fiberglass was SiO_2, with a
328 few other elements present (**Figure S10D**).

329

330 **Figure 3A** illustrates the mechanical mixing technique employed to produce the
331 hollow silica – fiberglass composite soft ceramic, which produced a promising
332 crosslinked ceramic structure based on intimate contact between hollow silica
333 particles and fiberglass fibers. We employed a simple high-shear blender to disrupt
334 the fiberglass network and simultaneously assemble the hollow silica on the
335 fiberglass matrix. Meanwhile, we used a filtration method, similar to papermaking,
336 to produce the final dried composite, demonstrating the potential for cost-
337 effective, environmentally friendly and scalable production. No silica particles or
338 fiberglass was wasted in the manufacturing process, which enables to accurate
339 control of the silica to fiberglass ratio in final product.

340

341 In general, the silica particles serve as a binder to hold the network together, while
342 reducing direct contact between fibers and simultaneously reducing potential gas
343 transport in the composite mat. The fiberglass provided a scaffold for loading and
344 dispersing the hollow silica particles to create a monolithic structure. The
345 microscopic 3D intertwined networks and other detailed information of pure
346 fiberglass were given in **Figure 3B.** The SEM image in **Figure 3C-D** exhibit the
347 morphology of the hollow silica – fiberglass ceramics, demonstrating that both G-
348 SiO_2 and L-SiO_2 could achieve high dispersion and loading on the fiberglass
349 surface. In contrast, the C-SiO_2 failed to disperse well, due to its high density and

350 aggregation (**Figure 3E**). Also, **Figure S11** shows the FTIR spectra of G-SiO$_2$

351 particle, commercial C-08-F fiberglass, and the fabricated G-SiO$_2$ – fiberglass

352 composite ceramic. Typically, the peaks below 1200 cm^{-1} attribute to inorganic

353 bonds, and the peaks at 1416 cm^{-1} and 1639 cm^{-1} attribute to the surface -OH

354 groups.[54] There was no new peak appearing in the composite ceramic,

355 suggesting that no chemical bond was formed between hollow silica and

356 fiberglass, and the interactions between hollow silica and fiberglass was physical

357 adsorption.
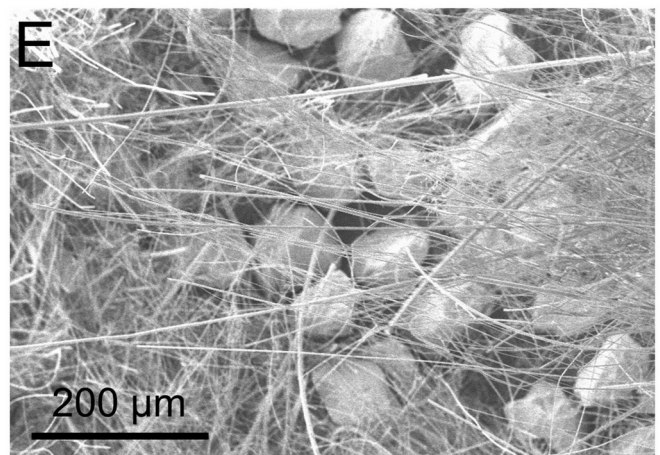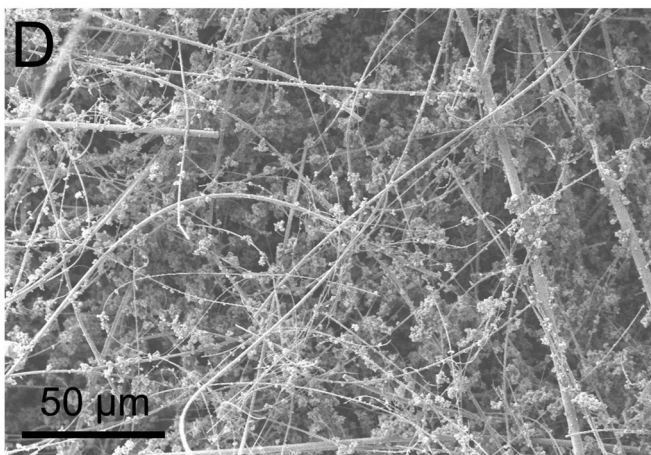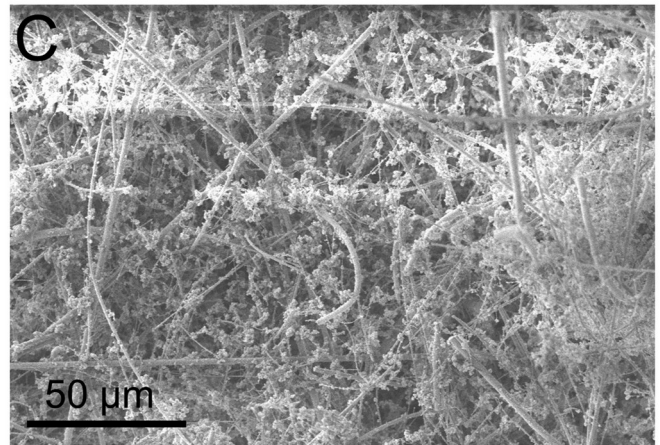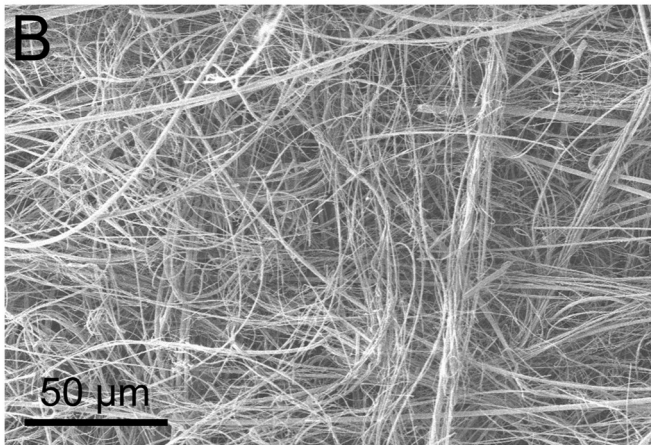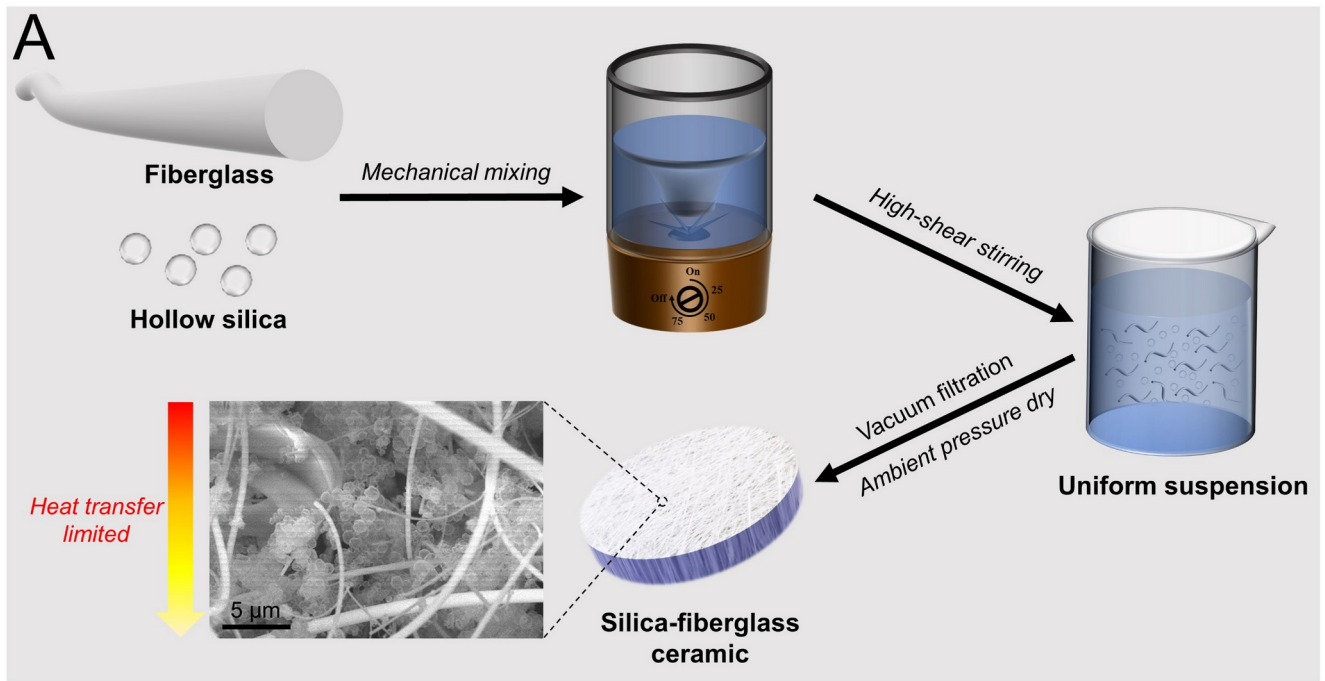
Figure 3. A. Manufacturing process and microscopic structure of the hollow silica – fiberglass composite ceramic. SEM images of **B.** commercial fiberglass, **C.** G-SiO$_2$ – fiberglass composite, **D.** L-SiO$_2$ – fiberglass composite, and **E.** C-SiO$_2$ – fiberglass composite.

Thermal transport can occur by convection, radiation and conduction, and the

effective thermal conductivity can be expressed as $k = k_s + k_g + k_c + k_r$, where k_s

365 and k_g are the solid and gaseous heat conduction, respectively; k_c is heat

366 convection which becomes negligible when the void size is smaller than 4 mm; k_r

367 is heat radiation which is proportional to T^3 and can also be ignored at room

368 temperature.[16, 56, 57] We further address how the obtained crosslinked hollow

369 silica – fiberglass structure contributes to reduce thermal conductivity, specifically

370 for the depressed k_s and k_g. As shown in **Figure 4A**, for the fiberglass without

371 hollow silica loading, heat conduction between fibers was smooth. After loading

372 hollow silica particles, with the interrupted void space between fibers, k_g

373 decreased due to the hollow void inside the silica particles and the void space in

374 the fiber network, which obviously increased the air molecules collision frequency.

375 Simultaneously, k_s was also limited because the heat transfer route in the solid

376 phase through the fiber network was interrupted by the hollow silica nanoshell on

377 surface. Such a frequently interrupting and alternating "solid-gas-solid-..." heat

378 transport mechanism leads to high thermal insulation performance of hollow silica

379 – fiberglass ceramics.

380

381 **Figure 4B** shows the thermal conductivity of the nanocomposite insulation with

382 varied silica content. When incorporating 20 wt.% G-SiO$_2$, the thermal conductivity

383 greatly reduced from 0.038 W/(m K) to 0.025 W/(m K), demonstrating the validity

384 of the proposed thermal insulation mechanism. The lowest thermal conductivity of

385 0.023 W/(m K) was realized at 60 wt.% G-SiO$_2$ content, and further increasing the

386 G-SiO$_2$ content to 80 wt.% increased the thermal conductivity. The L-SiO$_2$–

387 fiberglass ceramic obtained the lowest thermal conductivity of 0.026 W/(m K) at

388 50 wt.% L-SiO$_2$ content. Both G-SiO$_2$ – fiberglass and L-SiO$_2$ – fiberglass ceramics

389 provided better thermal insulation performance than C-SiO$_2$ – fiberglass ceramic

390 due to their natural low thermal conductivity and the good dispersion on

fiberglass. It's noticed that even the C-SiO$_2$ – fiberglass ceramic presented a thermal conductivity of 0.033 W/(m K), which was lower than that of either the fiberglass alone (0.038 W/(m K)) or the C-SiO$_2$ alone (0.046 W/(m K)), illustrating the generality of the technique applied in this work for manufacturing a class of thermal insulation materials. The thermal conductivity increased upon further increasing the silica content to 80 wt.%, which might be related to the increased density.

We further studied the relationship between the thermal conductivity and ceramic density with 50 wt.% silica content. The low density was achieved by a shorter filtration time, and the high density was achieved by thermal compression treatment in a tablet machine at 150 ºC. As shown in **Figure 4C**, the thermal conductivity exhibited a tendency of first decreasing and then increasing with increasing density. Here, we explained that the ceramic with low density had a large air space for effective heat transfer in gas phase. Slightly increasing the density could reduce the air space and thus limit the air molecules movement to reduce gas thermal conductivity. However, as shown in the third schematic in **Figure 4A**, further increasing the density increased the solid contacts, which introduced new heat transfer routes in the solid phase and caused the thermal conductivity to increase.

413
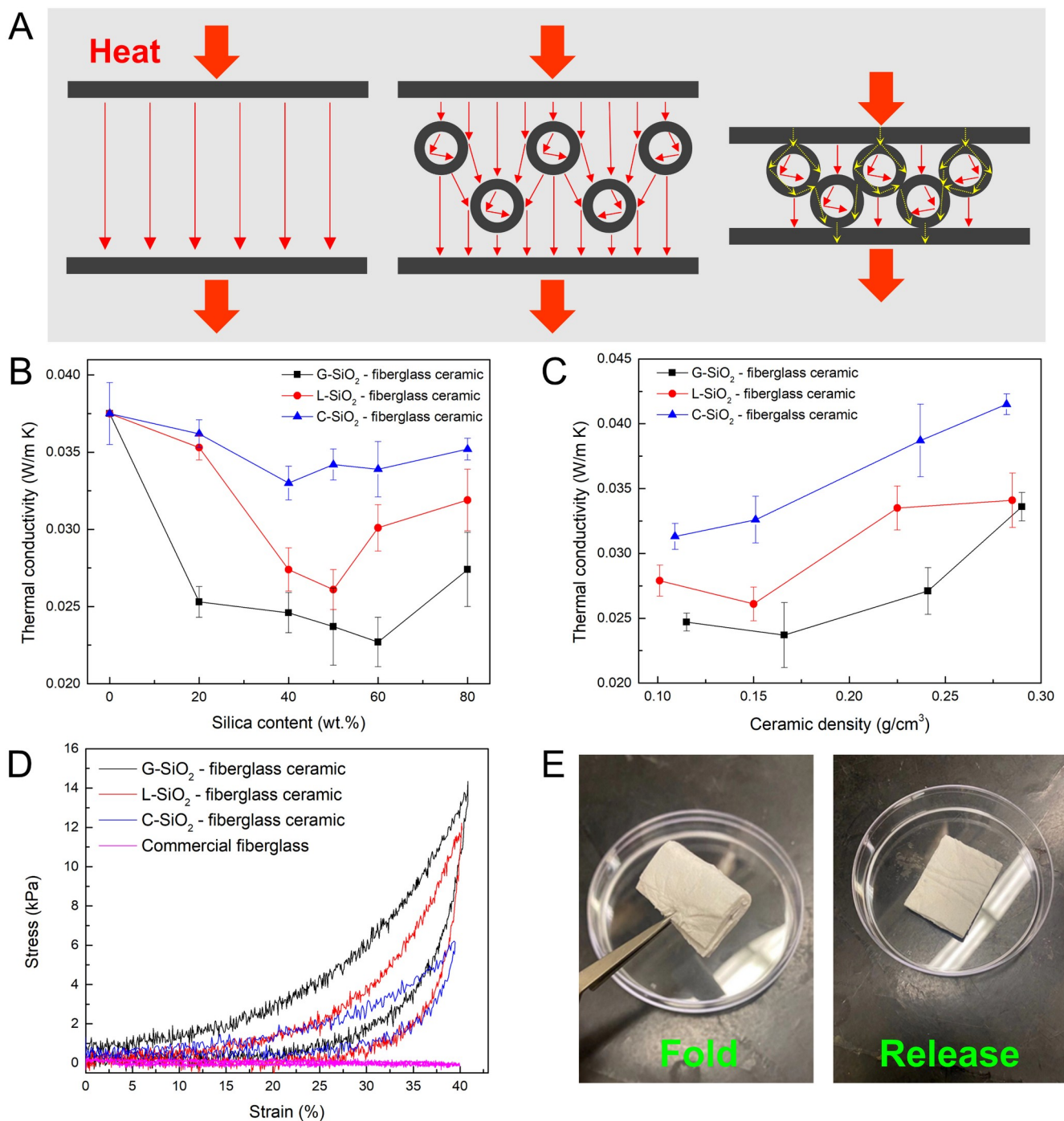
Figure 4. A. Schematic of heat conduction in the hollow silica – fiberglass ceramics. **B.** Thermal conductivity of hollow silica – fiberglass ceramics with varied silica content. **C.** Thermal conductivity of hollow silica – fiberglass ceramics with varied ceramic density. **D.** Engineering stress-strain curves of G-SiO$_2$ – fiberglass, L-SiO$_2$ – fiberglass, C-SiO$_2$ – fiberglass composite ceramics, and commercial fiberglass with 40% compressive strain. **E.** Ceramic folding to illustrate the mechanical flexibility of G-SiO$_2$ – fiberglass soft ceramic.

The interactions between hollow silica and fiberglass not only contribute to the

improved thermal insulation performance, but also the enhanced mechanical

properties, overcoming the intrinsically brittle characteristics of aerogel ceramics. After incorporation of hollow silica particles, the interfacial interaction among the fragile and loose state of original commercial fiberglass (**Figure S10B**) was enhanced. The silica particles provided a reinforcing effect on the fiber network, forming a block soft ceramic. To evaluate the elasto-flexibility, we performed the dynamic compression-recovery deformation tests and the correlated stress-strain curves of the soft ceramics, as shown in **Figure 4D**. The loading and unloading processes presented highly nonlinear behavior, and the stress-strain curves showed a closed hysteresis loop with no abrupt changes. These are the features of energy dissipative, elastic, and highly flexible materials.[8, 58] The Young's modulus of the $G-SiO_2$, $L-SiO_2$, and $C-SiO_2$ - fiberglass ceramics were 35 kPa, 30 kPa, and 15 kPa, respectively, indicating the robust elasticity of this class of materials. The Young's modulus of the commercial fiberglass, without processing or addition of hollow silica is too low to measure in the same configuration (**Figure 4C**, **Figure S10B**). We note that the Young's modulus of $G-SiO_2$ and $L-SiO_2$ – fiberglass soft ceramics were much higher than $C-SiO_2$ – fiberglass ceramics, which we attribute to the good dispersion of the silica particles within the fiber network. The well dispersed hollow silica particles reinforce the fiber scaffold to resist the compression force and enhance the mechanical strength of fabricated soft ceramics. As a typical example, **Figure 4E** illustrates the recoverable bending behavior of the $G-SiO_2$ – fiberglass soft ceramic, where the flexible ceramic material could be folded and unfolded without obvious structural damage. In addition, representative thermal images of the nanocomposites are provided in **Figure 5A-C**, showing the significant temperature gradient across samples with a thickness of 6 mm. As expected, the ceramics fabricated using $G-SiO_2$ and $L-SiO_2$ exhibited better thermal insulation property than $C-SiO_2$, which was in line with the

thermal conductivity analysis discussed above. **Figure 5D-F** illustrates the qualitative fire-retardant performance of composite ceramics in contact with an alcohol flame, confirming the potential applications in high temperature thermal insulation and fire protection.
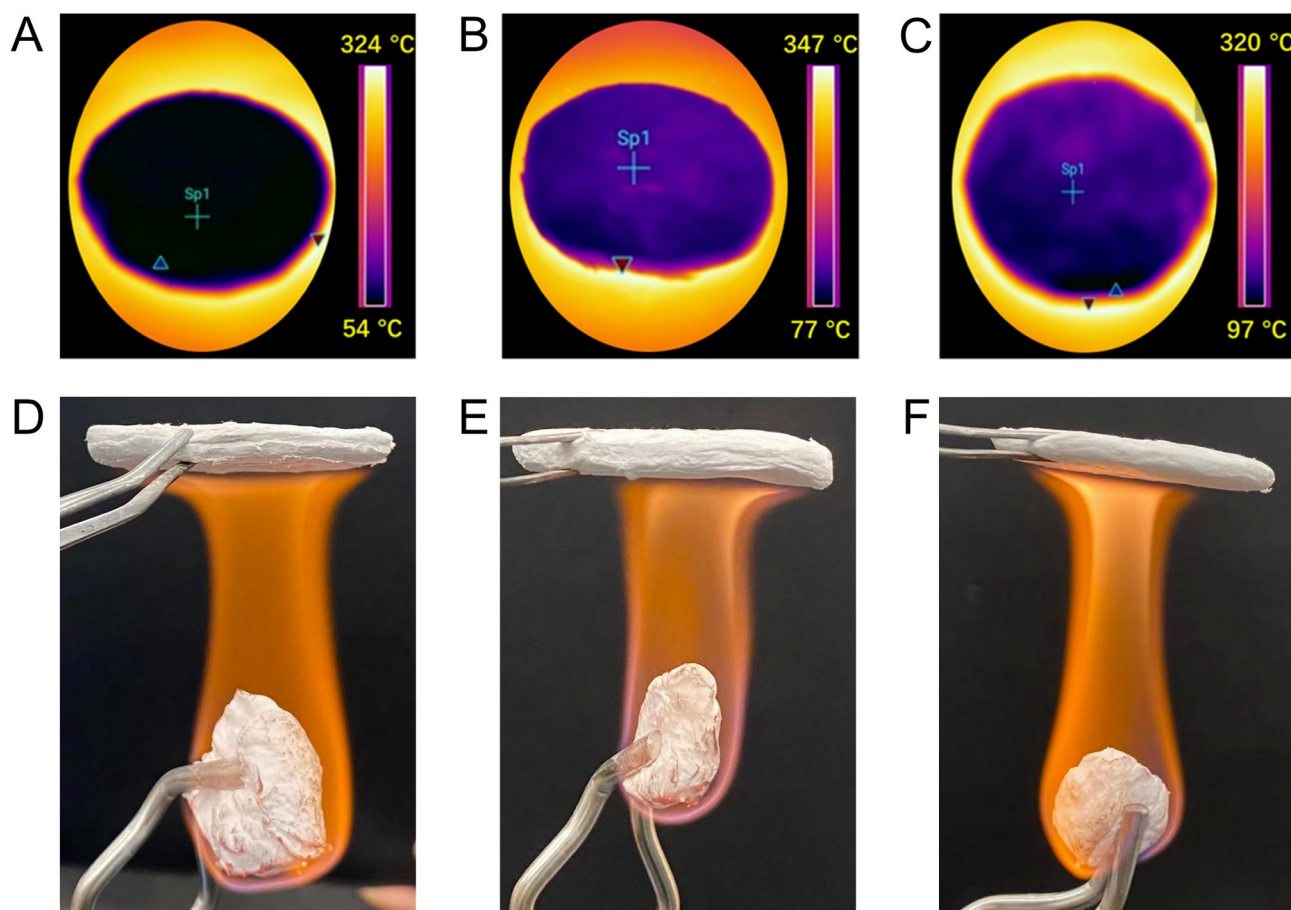
Figure 5. Infrared images of **A.** G-SiO$_2$, **B.** L-SiO$_2$, and **C.** C-SiO$_2$ – fiberglass ceramics (6 mm thickness, lowest thermal conductivity) on a 360 ºC hot plate at steady state. Optical images to illustrate the fire-retardancy of **D.** G-SiO$_2$ – fiberglass, **E.** L-SiO$_2$ – fiberglass and **F.** C-SiO$_2$ – fiberglass soft ceramics.

Finally, **Table 2** compares the manufacturing techniques and thermal conductivity of some reported hollow silica thermal insulation materials to evaluate their potential for scale-up and commercialization. As can be seen, for most of the hollow silica materials produced by hard template method with polystyrene microbeads as sacrificial template, although low thermal conductivity close to that of silica aerogels can be realized, the expensive price of polystyrene microbeads

467 (*e.g.* $260 for 0.5 g) impedes their practical use. In contrast, the present hollow

468 silica methods obtained similar or better thermal conductivity but adopted low-

469 cost raw materials and fewer manufacturing steps. On the other hand, silica

470 assembly methods include sintering to porous ceramics, and mixing into polymer

471 or fiberglass matrixes.[5] The porous ceramics involve high temperature

472 calcination procedure, and suffer from their stiff and fragile structure. Embedded

473 silica particles into fiber or other matrixes often requires complex fabrication

474 procedures and devices, such as electrospinning and 3D printing, which often face

475 barrier when scale-up, and the polymer matrixes are not capable of high

476 temperature and fire conditions. On the contrary, the high-shear mechanical

477 mixing technique proposed in current study only involves simple blending,

478 filtration, and drying procedures, without any complex devices, energy intensive

479 processing, or organic chemicals required. Meanwhile, the prepared thermal

480 insulation ceramics (or films) in **Table 2** show a broad range of thermal

481 conductivity, in where the thermal conductivity of G-SiO$_2$ – fiberglass and L-SiO$_2$ –

482 fiberglass soft ceramic are lower than most of the hollow silica insulation

483 materials, with robust mechanical properties and fire resistance, suggesting that it

484 is a promising method for scalable and low cost production of high performance

485 thermal insulation materials.

486

487

488

489

490

491

492

493

494

495

496

497

498

499

500

Table 2. Comparison of reported hollow silica thermal insulation materials

Category	Raw material	Fabrication method	K (W m^{-1} K^{-1})	Ref.
Hollow silica particle	Polystyrene microbeads, TEOS, EtOH, H_2O, NH_4OH	Hard template	0.020	[38]
	Polystyrene microbeads, TEOS, EtOH, H_2O, NH_4OH	Hard template	0.035	[15]
	Polystyrene microbeads, TEOS, EtOH, H_2O, NH_4OH	Hard template	0.015	[14]
	CTAB, TEOS, EtOH, H_2O, HCl	Flame aerosol process	0.023	This study
	Carbon particles, TEOS, EtOH, H_2O, NH_4OH	Hard template	0.025	This study
Hollow silica ceramic	Hollow SiO_2, acrylamide, ammonium persulfate, …	Sintering	0.102	[39]
	Hollow SiO_2, MTMS, cyclohexane, EtOH, H_2O, HCl	Sol-gel process	0.031	[59]
	Hollow glass, TEOS, oxalic acid, EtOH, H_2O, DMF, NH_4OH	Pressing and sintering; Sol-gel process	0.033	[60]
	TEOS, CTAB, urea, acetic acid, H_2O	Sol-gel process; Thermal annealing	0.036	[49]
	Hollow SiO_2, H_2O	Thermal annealing	0.071	[37]
Hollow silica-polymer composite film	PU, hollow SiO_2, EtOH	Surface modification; Solvent evaporation	0.050	[41]
	PU, hollow SiO_2, EtOH	Surface modification; Spray coating	0.029	[61]
	PES, hollow SiO_2, DMAc	Film coating	0.030	[17]
	PVDF, epoxy, hollow glass,	Spin coating/gravure	0.047	[62]

	NMP	printing		
	Silicone rubber, hollow SiO_2	Casting; polymerization	0.149	[42]
	PAN, hollow SiO_2, DMF	Electrospinning	0.016	[47]
	PVP, PVA, hollow SiO_2, NH_4OH, …	Electrospinning	0.023	[46]
Hollow silica-fiberglass composite ceramic	Fiberglass, PU, hollow glass	Coating	0.115	[63]
	Fiberglass, hollow glass, nano-SiO_2, sepiolite fiber	Mechanical mixing; Solvent evaporation	0.050	[64]
	Fiberglass, Hollow L-SiO_2, H_2O	Mechanical mixing	0.026	This study
	Fiberglass, Hollow G-SiO_2, H_2O	Mechanical mixing	0.023	This study

501

502

503

504

Conclusions

In summary, we present two facile routes to produce hollow silica thermal insulation materials in both gas-phase and liquid-phase, which provide superior performance attributes such as low density, high porosity, and low thermal conductivity. Furthermore, we present a high shear mechanical mixing and filtration method for fabrication of hollow silica – fiberglass composite soft ceramics. Both the thermal insulation and mechanical performance could be enhanced by the crosslinked network structure, demonstrating a low thermal conductivity of 0.023 W/(m K) and robust elasto-flexibility. This soft ceramic manufacturing technology can be extended to other aerogel-fiber systems as well to broaden their applications, potentially enabling scalable, low-cost, and environmentally friendly fabrication of energy saving and thermal protection materials.

518

Conflicts of interest

520 The authors have no conflicts to declare.

521

Acknowledgements

528

529

530

531

References

533 [1] W. Villasmil, L.J. Fischer, J. Worlitschek, A review and evaluation of thermal
534 insulation materials and methods for thermal energy storage systems, Renew.
535 Sust. Energ. Rev., 103 (2019) 71-84.
536
537 [2] E. Cuce, P.M. Cuce, C.J. Wood, S.B. Riffat, Toward aerogel based thermal
538 superinsulation in buildings: A comprehensive review, Renew. Sust. Energ. Rev., 34
539 (2014) 273-299.
540
541 [3] N. Hüsing, U. Schubert, Aerogels—airy materials: chemistry, structure, and
542 properties, Angew. Chem.-Int. Edit., 37 (1998) 22-45.
543
544 [4] P.C. Thapliyal, K. Singh, Aerogels as promising thermal insulating materials: An
545 overview, J. Mater, 2014 (2014).
546
547 [5] T. Linhares, M.T.P. de Amorim, L. Durães, Silica aerogel composites with
548 embedded fibres: a review on their preparation, properties and applications,
549 Journal of Materials Chemistry A, 7 (2019) 22768-22802.
550
551 [6] X. Zhang, X. Ni, C. Li, B. You, G. Sun, Co-gel strategy for preparing
552 hierarchically porous silica/polyimide nanocomposite aerogel with thermal

insulation and flame retardancy, J. Mater. Chem. A, 8 (2020) 9701-9712.

[7] X. Xu, Q. Zhang, M. Hao, Y. Hu, Z. Lin, L. Peng, T. Wang, X. Ren, C. Wang, Z. Zhao, Double-negative-index ceramic aerogels for thermal superinsulation, Science, 363 (2019) 723-727.

[8] L. Li, C. Jia, Y. Liu, B. Fang, W. Zhu, X. Li, L.A. Schaefer, Z. Li, F. Zhang, X. Feng, N. Hussain, X. Xi, D. Wang, Y.H. Lin, X. Wei, H. Wu, Nanograin–glass dual-phasic, elasto-flexible, fatigue-tolerant, and heat-insulating ceramic sponges at large scales, Mater. Today, 54 (2022) 72-82.

[9] X. Wu, M. Fan, J.F. Mclaughlin, X. Shen, G. Tan, A novel low-cost method of silica aerogel fabrication using fly ash and trona ore with ambient pressure drying technique, Powder Technol., 323 (2018) 310-322.

[10] Y.F. Lin, C.R. Syu, K.W. Huang, K.Y.A. Lin, Synthesis of silica aerogel membranes using low-cost silicate precursors for carbon dioxide capture, Chem. Phys. Lett., 726 (2019) 13-17.

[11] L. An, D. Petit, M. Di Luigi, A. Sheng, Y. Huang, Y. Hu, Z. Li, S. Ren, Reflective Paint Consisting of Mesoporous Silica Aerogel and Titania Nanoparticles for Thermal Management, ACS Appl. Nano Mater., 4 (2021) 6357-6363.

[12] L. An, M. Di Luigi, D. Petit, Y. Hu, Y. Chen, J.N. Armstrong, Y.C. Li, S. Ren, Nanoengineering Porous Silica for Thermal Management, ACS Appl. Nano Mater., 5.2 (2022) 2655-2663.

[13] S. Liu, M. Shah, S. Rao, L. An, M.M. Mohammadi, A. Kumar, S. Ren, M.T. Swihart, Flame aerosol synthesis of hollow alumina nanoshells for application in thermal insulation, Chem. Eng. J., 428 (2022) 131273.

[14] Y. Liao, X. Wu, H. Liu, Y. Chen, Thermal conductivity of powder silica hollow spheres, Thermochim. Acta, 526 (2011) 178-184.

[15] P. Ruckdeschel, A. Philipp, M. Retsch, Understanding Thermal Insulation in Porous, Particulate Materials, Adv. Funct. Mater., 27.38 (2017) 1702256.

[16] F. Hu, S. Wu, Y. Sun, Hollow-Structured Materials for Thermal Insulation, Adv. Mater., 31.38 (2019) 1801001.

[17] L. Ernawati, T. Ogi, R. Balgis, K. Okuyama, M. Stucki, S.C. Hess, W.J. Stark, Hollow Silica as an Optically Transparent and Thermally Insulating Polymer Additive, Langmuir, 32 (2016) 338-345.

[18] W. Cui, T. Wang, A. Yan, S. Wang, Superamphiphobic surfaces constructed by cross-linked hollow SiO_2 spheres, Appl. Surf. Sci., 400 (2017) 162-171.

[19] L. Han, C. Gao, X. Wu, Q. Chen, P. Shu, Z. Ding, S. Che, Anionic surfactants templating route for synthesizing silica hollow spheres with different shell porosity, Solid State Sci., 13 (2011) 721-728.

[20] Q. Yu, P. Wang, S. Hu, J. Hui, J. Zhuang, X. Wang, Hydrothermal synthesis of

hollow silica spheres under acidic conditions, Langmuir, 27 (2011) 7185-7191.

[21] S.H. Wu, C.Y. Mou, H.P. Lin, Synthesis of mesoporous silica nanoparticles, Chem. Soc. Rev., 42 (2013) 3862-3875.

[22] R. Koirala, S.E. Pratsinis, A. Baiker, Synthesis of catalytic materials in flames: opportunities and challenges, Chem. Soc. Rev., 45 (2016) 3053-3068.

[23] C. Boissiere, D. Grosso, A. Chaumonnot, L. Nicole, C. Sanchez, Aerosol route to functional nanostructured inorganic and hybrid porous materials, Adv. Mater., 23 (2011) 599-623.

[24] M. Malekzadeh, M.T. Swihart, Vapor-phase production of nanomaterials, Chem. Soc. Rev., 50.12 (2021) 7132-7249.

[25] D.P. Debecker, S. Le Bras, C. Boissiere, A. Chaumonnot, C. Sanchez, Aerosol processing: a wind of innovation in the field of advanced heterogeneous catalysts, Chem. Soc. Rev., 47 (2018) 4112-4155.

[26] F. Colbeau-Justin, C. Boissière, A. Chaumonnot, A. Bonduelle, C. Sanchez, Aerosol Route to Highly Efficient (Co)Mo/SiO_2 Mesoporous Catalysts, Adv. Funct. Mater., 24 (2014) 233-239.

[27] K. Kho, K. Hadinoto, Aqueous re-dispersibility characterization of spray-dried hollow spherical silica nano-aggregates, Powder Technol., 198 (2010) 354-363.

[28] Z.X. Wu, K. Waldron, X.C. Zhang, Y.Q. Li, L. Wu, W.D. Wu, X.D. Chen, D.Y. Zhao, C. Selomulya, Spray-drying water-based assembly of hierarchical and ordered mesoporous silica microparticles with enhanced pore accessibility for efficient bio-adsorption, J. Colloid Interface Sci., 556 (2019) 529-540.

[29] W.S. Cheow, S. Li, K. Hadinoto, Spray drying formulation of hollow spherical aggregates of silica nanoparticles by experimental design, Chem. Eng. Res. Des., 88 (2010) 673-685.

[30] E.C. Lovell, H. Grossman, J. Horlyck, J. Scott, L. Madler, R. Amal, Asymmetrical Double Flame Spray Pyrolysis-Designed SiO_2/$Ce_{0.7}Zr_{0.3}O_2$ for the Dry Reforming of Methane, ACS Appl. Mater. Interfaces, 11 (2019) 25766-25777.

[31] N.H. Paulson, J.A. Libera, M. Stan, Flame spray pyrolysis optimization via statistics and machine learning, Mater. Des., 196 (2020) 108972.

[32] H. Schulz, L. Madler, S.E. Pratsinis, P. Burtscher, N. Moszner, Transparent nanocomposites of radiopaque, flame-made Ta_2O_5/SiO_2 particles in an acrylic matrix, Adv. Funct. Mater., 15 (2005) 830-837.

[33] W.J. Scharmach, R.D. Buchner, V. Papavassiliou, P. Pacouloute, M.T. Swihart, A High-Temperature Reducing Jet Reactor for Flame-Based Metal Nanoparticle Production, Aerosol Sci. Technol., 44 (2010) 1083-1088.

[34] S. Liu, M.M. Mohammadi, M.T. Swihart, Fundamentals and recent applications of catalyst synthesis using flame aerosol technology, Chem. Eng. J., 405 (2021)

126958.

[35] M.M. Mohammadi, S. Shao, S. Srivatsa Gunturi, A.R. Raghavan, N. Alexander, Y. Liu, C.M. Stafford, R.D. Buchner, M.T. Swihart, A general approach to multicomponent metal-decorated crumpled reduced graphene oxide nanocomposites using a flame-based process, Nanoscale, 11 (2019) 19571-19578.

[36] M.K. Sharma, D. Qi, R.D. Buchner, W.J. Scharmach, V. Papavassiliou, M.T. Swihart, Flame-driven Aerosol Synthesis of Copper-Nickel Nanopowders and Conductive Nanoparticle Films, ACS Appl. Mater. Interfaces, 6 (2014) 13542-13551.

[37] P. Ruckdeschel, T.W. Kemnitzer, F.A. Nutz, J. Senker, M. Retsch, Hollow silica sphere colloidal crystals: insights into calcination dependent thermal transport, Nanoscale, 7 (2015) 10059-10070.

[38] T. Gao, B.P. Jelle, L.I.C. Sandberg, A. Gustavsen, Monodisperse Hollow Silica Nanospheres for Nano Insulation Materials: Synthesis, Characterization, and Life Cycle Assessment, ACS Appl. Mater. Interfaces, 5 (2013) 761-767.

[39] Z. Sun, C. Lu, J. Fan, F. Yuan, Porous silica ceramics with closed-cell structure prepared by inactive hollow spheres for heat insulation, J. Alloys Compd., 662 (2016) 157-164.

[40] A. Lai, Z. Du, C.L. Gan, C.A.J.S. Schuh, Shape memory and superelastic ceramics at small scales, Science, 341 (2013) 1505-1508.

[41] Y. Liao, X. Wu, Z. Wang, R. Yue, G. Liu, Y. Chen, Composite thin film of silica hollow spheres and waterborne polyurethane: Excellent thermal insulation and light transmission performances, Mater. Chem. Phys., 133 (2012) 642-648.

[42] X.-W. Zhao, C.-G. Zang, Y.-L. Sun, Y.-L. Zhang, Y.-Q. Wen, Q.-J. Jiao, Effect of hybrid hollow microspheres on thermal insulation performance and mechanical properties of silicone rubber composites, J. Appl. Polym. Sci., 135.11 (2018) 46025.

[43] X. Mao, J. Hong, Y.X. Wu, Q. Zhang, J. Liu, L. Zhao, H.H. Li, Y.Y. Wang, K. Zhang, An Efficient Strategy for Reinforcing Flexible Ceramic Membranes, Nano Lett., 21 (2021) 9419-9425.

[44] L. An, J.N. Armstrong, Y. Hu, Y. Huang, Z. Li, D. Zhao, J. Sokolow, Z. Guo, C. Zhou, S. Ren, High temperature ceramic thermal insulation material, Nano Res., (2022) 1-8.

[45] L. An, B. Liang, Z. Guo, J. Wang, C. Li, Y. Huang, Y. Hu, Z. Li, J.N. Armstrong, C. Zhou, D. Faghihi, S. Ren, Wearable Aramid–Ceramic Aerogel Composite for Harsh Environment, Adv. Eng. Mater., 23.3 (2021) 2001169.

[46] B. Zhang, Z. Tong, Y. Pang, H. Xu, X. Li, H. Ji, Design and electrospun closed cell structured SiO2 nanocomposite fiber by hollow SiO_2/TiO_2 spheres for thermal insulation, Compos. Sci. Technol., 218 (2022) 109152.

[47] D. Tao, X. Li, Y. Dong, Y. Zhu, Y. Yuan, Q. Ni, Y. Fu, S. Fu, Super-low thermal conductivity fibrous nanocomposite membrane of hollow silica/polyacrylonitrile,

Compos. Sci. Technol., 188 (2020) 107992.

[48] S. Liu, C. Dun, J. Chen, S. Rao, M. Shah, J. Wei, K. Chen, Z. Xuan, E.A. Kyriakidou, J.J. Urban, M.T. Swihart, A General Route to Flame Aerosol Synthesis and In Situ Functionalization of Mesoporous Silica, Angew. Chem. Int. Ed. Engl., (2022) e202206870.

[49] R. Yang, F. Hu, L. An, J. Armstrong, Y. Hu, C. Li, Y. Huang, S. Ren, A Hierarchical Mesoporous Insulation Ceramic, Nano Lett., 20 (2020) 1110-1116.

[50] X. Ma, Z. Wei, H. Han, X. Wang, K. Cui, L. Yang, Tunable construction of multi-shell hollow SiO_2 microspheres with hierarchically porous structure as high-performance anodes for lithium-ion batteries, Chem. Eng. J., 323 (2017) 252-259.

[51] Y. Si, J.Y. Yu, X.M. Tang, J.L. Ge, B. Ding, Ultralight nanofibre-assembled cellular aerogels with superelasticity and multifunctionality, Nat. Commun., 5.1 (2014) 1-9.

[52] K. Li, J. Wei, H. Yu, P. Xu, J. Wang, H. Yin, M.A. Cohen Stuart, J. Wang, S. Zhou, A Generic Method for Preparing Hollow Mesoporous Silica Catalytic Nanoreactors with Metal Oxide Nanoparticles inside Their Cavities, Angew. Chem. Int. Ed. Engl., 57 (2018) 16458-16463.

[53] L. An, D. Zhang, L. Zhang, G. Feng, Effect of nanoparticle size on the mechanical properties of nanoparticle assemblies, Nanoscale, 11 (2019) 9563-9573.

[54] S. Liu, X. Chen, W. Ai, C. Wei, A new method to prepare mesoporous silica from coal gasification fine slag and its application in methylene blue adsorption, J. Clean Prod., 212 (2019) 1062-1071.

[55] T. Linhares, M.T. Pessoa de Amorim, L. Durães, Silica aerogel composites with embedded fibres: a review on their preparation, properties and applications, J. Mater. Chem. A, 7 (2019) 22768-22802.

[56] T. Xie, Y.-L. He, Z.-J. Hu, Theoretical study on thermal conductivities of silica aerogel composite insulating material, Int. J. Heat Mass Transfer, 58 (2013) 540-552.

[57] J.-J. Zhao, Y.-Y. Duan, X.-D. Wang, B.-X. Wang, Radiative properties and heat transfer characteristics of fiber-loaded silica aerogel composites for thermal insulation, Int. J. Heat Mass Transfer, 55 (2012) 5196-5204.

[58] H.-J. Zhan, K.-J. Wu, Y.-L. Hu, J.-W. Liu, H. Li, X. Guo, J. Xu, Y. Yang, Z.-L. Yu, H.-L. Gao, Biomimetic carbon tube aerogel enables super-elasticity and thermal insulation, Chem, 5 (2019) 1871-1882.

[59] M. Grandcolas, E. Jasinski, T. Gao, B.P. Jelle, Preparation of low density organosilica monoliths containing hollow silica nanospheres as thermal insulation materials, Mater. Lett., 250 (2019) 151-154.

[60] J. Ding, Q. Liu, B. Zhang, F. Ye, Y. Gao, Preparation and characterization of hollow glass microsphere ceramics and silica aerogel/hollow glass microsphere

ceramics having low density and low thermal conductivity, J. Alloys Compd., 831 (2020) 154737.

[61] M. Fuji, C. Takai, H. Watanabe, K. Fujimoto, Improved transparent thermal insulation using nano-spaces, Adv. Powder Technol., 26 (2015) 857-860.

[62] Z. Wang, T. Zhang, B.K. Park, W.I. Lee, D.J. Hwang, Minimal contact formation between hollow glass microparticles toward low-density and thermally insulating composite materials, J. Mater. Sci., 52 (2017) 6726-6740.

[63] J. Sun, F. Cai, D. Tao, Q. Ni, Y. Fu, Enhanced Thermal Insulation of the Hollow Glass Microsphere/Glass Fiber Fabric Textile Composite Material, Polymers (Basel), 13.4 (2021) 505.

[64] S. Xu, L. Chen, M. Gong, X. Hu, X. Zhang, Z. Zhou, Characterization and engineering application of a novel ceramic composite insulation material, Compos. Pt. B-Eng., 111 (2017) 143-147.